Improved spectral characteristics of 980 nm broad area slotted Fabry–Perot diode lasers*

Gao Zhuo(高卓)†, Wang Jun(王俊), Xiong Cong(熊聪), Liu Yuanyuan(刘媛媛), Liu Suping(刘素平), and Ma Xiaoyu(马骁宇)

Institute of Semiconductors, Chinese Academy of Sciences, Beijing 100083, China

Abstract: A novel broad area slotted Fabry–Perot diode laser is designed and fabricated. Using a new semi-analytical method, we introduce effective refractive index perturbations in the form of etched slot features into a conventional 980 nm broad area Fabry–Perot cavity, and the spectral characteristics of the device are expected to be noticeably improved. A low density of slot features is formed by using standard optical lithography and inductively coupled plasma dry etching. The experimental results show that the full spectral width at half-maximum is less than 0.4 nm, meanwhile, the thermal shift of the emission spectrum is decreased from 0.26 to 0.07 nm/℃ over a temperature range of 10 to 60 ℃. The improved spectral characteristics of the device are proved to be attributed to such slotted Fabry–Perot laser structures.

Key words: broad area diode lasers; slot features; spectral width; wavelength stabilization

DOI: 10.1088/1674-4926/33/1/014007 **PACC:** 4260B; 4260D; 7850G

1. Introduction

High-power diode lasers operating at wavelengths around 980 nm are widely used for pumping Yb-doped fiber lasers as well as Er-doped fiber lasers and amplifiers owing to their excellent absorption and improved efficiency. However, the narrow pumping absorption bandwidth at around 980 nm (only 5–9 nm FWHM)[1] challenges the spectral characteristics of the pump source because conventional broad-area (BA) Fabry–Perot (FP) diode lasers exhibit a considerable spectral shift with both temperature and operating current. Therefore, it is crucial to realize narrow linewidth and wavelength stability of the pump spectrum.

To date, there are many common methods to realize both single-mode emission and wavelength stabilization of the pump lasers, such as distributed feedback (DFB), external cavity feedback including volume holographic grating (VHG) as well as volume Bragg grating (VBG), etc. However, DFB requires complex process and regrowth steps and VBG is highly sensitive to collimation so neither of these devices is fit for mass-manufacture applications. Therefore we need to consider an alternative approach to satisfy increasing demand for easier fabrication process and superior reliability.

In recent years, researchers have found that effective index perturbations introduced by etching slot features along the ridge waveguide FP cavity can dramatically improve the spectral purity[2–4] and wavelength stabilization[5] of the FP diode laser emitting in the long wavelength range. In order to meet a further requirement for wavelength-stabilized pump lasers with a higher output power, we attempt here to integrate such a new approach[6] into conventional FP lasers at a 980 nm wavelength and develop a novel 980 nm BA slotted FP laser. The devices are expected to realize narrow spectral width and superior temperature stability.

2. Theory and design

More recently, O'Brien provided a semi-analytical approach[6] that put up a straightforward bridge between spectral manipulation for a given wavelength and a spatially distribution of varying effective refractive index in the form of slot features along the FP cavity. Such a spatially varying refractive index in a one-dimensional system is shown in Fig. 1. We assume that the effective refractive index step Δn is real and small enough relative to the cavity effective index n, i.e. $\Delta n \ll n$, the threshold gain g_{th} of the mth cavity resonance in wavenumber space can be deduced in terms of $m = m_0 + \Delta m$ as follows[6]:

$$g_{\text{th}} = g_{\text{th0}} + \frac{\Delta n}{n} \Delta g_{\text{th}}, \tag{1}$$

$$g_{\text{th0}} = 1/L_{\text{c}} \ln(1/|r_1 r_2|), \tag{2}$$

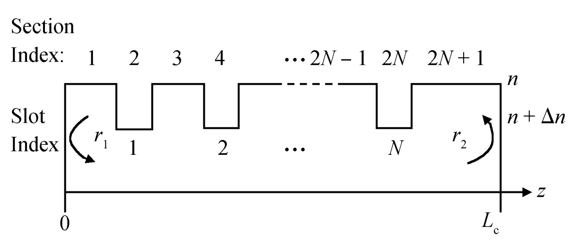

Fig. 1. Schematic diagram of the longitudinal section along a slotted FP laser cavity. The length of cavity with $2N + 1$ sections and N slot features is L_{c}. The effective index of the FP cavity is n and that of the slotted region is $n + \Delta n$. The complex facet reflectivities are r_1 and r_2, respectively.

* Project supported by the Knowledge Innovation Program of the Chinese Academy of Sciences (No. ISCAS2008T12).
† Corresponding author. Email: gaozh@semi.ac.cn
Received 11 July 2011
© 2012 Chinese Institute of Electronics

Table 1. Parameters of the device at 980 nm wavelength.

Parameter	Value
λ	980 nm
L_c	600 μm
n	3.3
Δn	-0.005
m_0	4040
a	60
τ	0.012

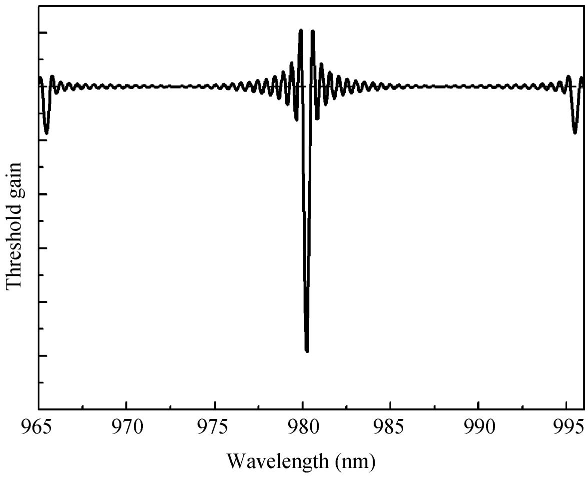

Fig. 2. Calculated threshold gain spectrum for the emitting wavelength around 980 nm. The horizontal line is at the value of the mirror loss of the plain FP cavity.

$$\Delta g_{\text{th}} \sim \exp\left[-\pi\tau^2(\Delta m)^2\right]\sum_{k=-\infty}^{\infty}\sin c(\Delta m - ka), \quad (3)$$

where g_{th0} is the threshold gain of the plain FP cavity for the given cavity mode $m_0(\Delta n = 0)$, Δg_{th} is proportional to the amplitude of the threshold gain modulation introduced by low density refractive index perturbations($\Delta n \neq 0$), which can be approximately expressed by a periodic distribution of $\sin c$ functions with spacing a cavity modes by multiplying a Gaussian envelope function, where τ determines the decay of the Gaussian envelope corresponding to an 80% suppression of the threshold gain modulation at $\Delta m = \pm a$.

Based on the Fourier transform of the threshold gain modulation spectrum Eq. (3), the approximate slot feature positions are determined by[6]

$$C\sum_k \int_{x_{\min}}^{x_j} [f(x)]^{-1} \exp\left[-\pi/\tau^2(x-k/a)^2\right]\mathrm{d}x = j - 1/2, \quad (4)$$

where $f(x) = |r_1|\exp(xL_c g_{\text{th0}}) - |r_2|\exp(-xL_c g_{\text{th0}})$, x is the position of the slot center from the device center as a fraction of the cavity length, and $-1/2 \leqslant x \leqslant 1/2$. The slot features are numbered with an index j, $j = 1, 2, \cdots, N$ and C is normalized to the number of slots. When the approximate x_j are initially generated, the positions of slots should be corrected by the phase requirement $\sin(2\pi x_j m_0) = 1$ considering the slot features are only placed on the right side of the device center.

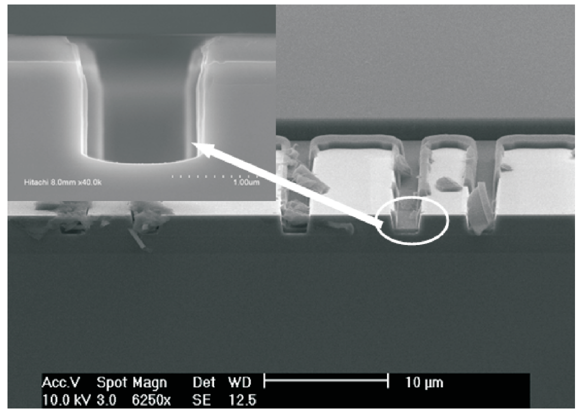

Fig. 3. An SEM profile section image of the etched slot features along the FP cavity. Inset: Cross-section of an etched slot feature.

For our case, the device parameters are given in Table 1 and the expected threshold gain spectrum of the slotted FP cavity is shown in Fig. 2. From Fig. 2, we find that the magnitude of the threshold gain modulation around 980 nm is markedly maximized compared to other adjacent modes, then excellent selectivity at $m = m_0$ is realized.

With $N = 6$ slots, the mirror reflectivities of uncoated facets are approximately 0.535, and $x_{\min} = 0.004$ considering a $\frac{\pi}{2}$ phase shift should be added to the distribution of slot features at the device center, then the central positions of slot features to the left facet can be finally determined by Eq. (4) as listed below: 304.2, 309.3, 319.5, 341.9, 391.5 and 500.8 μm.

3. Device fabrication

The epitaxial structures of the device are grown by low-pressure metal organic chemical vapor deposition (MOCVD) on an n-doped GaAs substrate. The active region consists of an AlGaInAs SQW with an emission wavelength at 980 nm embedded in a symmetrical AlGaAs waveguide, which is surrounded by n- and p-doped cladding layers as listed in Table 2. The slot features are formed in a 50-μm-wide BA stripe along the FP cavity by standard optical lithography and ICP dry etching technology, which don't involve epitaxial regrowth. An InGaP etch-stop layer is introduced into the upper cladding layer to precisely define the depth of the etched slots, considering high dry-etching selectivity of AlGaAs over InGaP in BCl_3/SF_6 discharge[7, 8]. After dry etching, wet chemical etching should be performed using a chemical solution of 1 : 1 : 10 $H_2SO_4 : H_2O_2 : H_2O$ cooled to 4 ℃[9] to improve surface cleanness and smoothness.

Each slot length is approximately 1 μm. The sidewalls of slots are passivated with SiO_2 and the openings are made to the top of the BA stripe, as shown in Fig. 3, where a patterned Ti/Pt/Au ohmic contact is prepared by using a magnetic sputtering technique. A Au/Ge/Ni/Au contact is evaporated on the n-type substrate. The wafer is cleaved to laser bars of the given cavity length without facet coating, and then laser bars are used to fabricate single emitters and the cleaved chips are mounted p-side down on copper heat sinks with indium solder for testing.

Table 2. Epitaxial structures of the AlGaInAs SQW laser with an InGaP etch-stop layer.

Layer name	Layer composition	Thickness (μm)	Doping concentration (p, n: 10^{18} cm^{-3})
Cap	GaAs	0.25	$p = 100$
Upper cladding_2	$Al_{0.42}Ga_{0.58}As$	1.2	$p = 2.0$
Etch-stop	InGaP	0.02	$p = 2.0$
Upper cladding_1	$Al_{0.42}Ga_{0.58}As$	0.3	$p = 2.0$
Upper waveguide	$Al_{0.22}Ga_{0.78}As$	0.1	Undoped
SQW	AlGaInAs	0.01	Undoped
Lower waveguide	$Al_{0.22}Ga_{0.78}As$	0.1	Undoped
Lower cladding	$Al_{0.42}Ga_{0.58}As$	1.5	$n = 1.0$

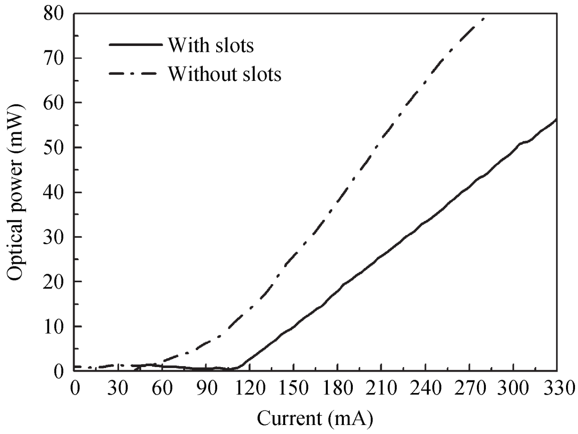

Fig. 4. Power–current characteristics for etched slots (solid) and no slots (dash dot) of broad area FP diode lasers at 20 ℃.

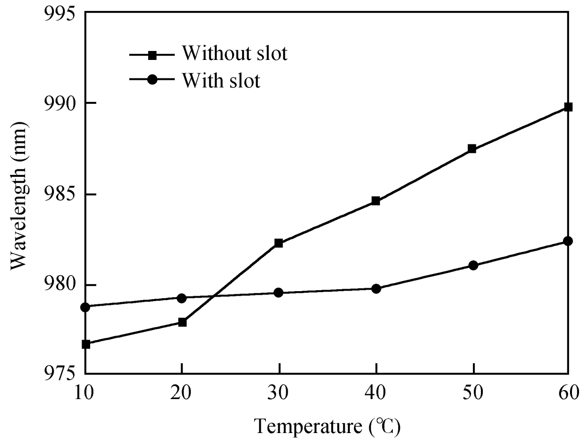

Fig. 6. Laser wavelength as a function of temperature with slots (circles) and without slot (squares) at $1.5I_{th}$.

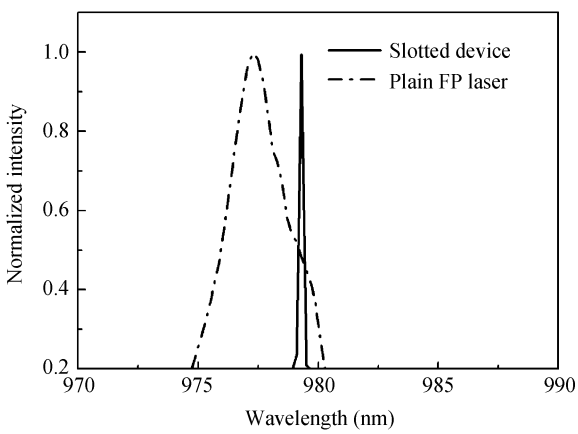

Fig. 5. Spectra of an etched slots device (solid) and an equivalent plain FP laser without slots (dash dot) on the same bar at $1.5I_{th}$.

4. Experimental results

The devices are tested under pulsed current operation (50 μs, 100 Hz). First we present the power–current characteristics at 20 ℃ as given in Fig. 4. The values of threshold current and output power at twice threshold without slot and with slots are 96 and 112 mA, and 46 and 32 mW, respectively. We see that the device with additional slots exhibits a slightly higher threshold current that can be attributed to some absorption or scattering losses introduced from slot features[6].

Figure 5 shows a comparison between the emission spectrum of a broad area FP laser with and without slots. Compared with a 4.6 nm FWHM of the plain FP device, the typical spectral width (FWHM) of a BA slotted FP laser is less than 0.4 nm and the center wavelength is 979.3 nm tested under pulse (50 μs, 100 Hz) operation at 20 ℃.

Figure 6 demonstrates the difference between the temperature stability of slotted devices and that of an equivalent plain FP cavity measured at $1.5I_{th}$ under continuous wave (CW) conditions. When the temperature varies from 10 to 60 ℃, we find that the device with slots exhibits much better wavelength stability than the no-slot device, even though the former shows a higher wavelength shift toward the infrared with a higher threshold current in the beginning. The center wavelength of the emission spectrum without slots and with slots is increased from 976.8 to 989.8 nm and 978.8 to 982.5 nm, respectively. The thermal shift of the spectrum is reduced from 0.26 to 0.07 nm/℃.

The above experimental results have proved that the BA slotted FP laser structure can narrow the emission spectrum at wavelengths around 980 nm as well as improve the spectral stability in comparison with the equivalent plain FP laser.

5. Conclusions

We have presented how to introduce a novel effective index patterns into conventional 980 nm broad area Fabry–Perot diode lasers. In this letter, slot features are formed by using standard optical lithography and ICP dry etching. This fabrication process results in lower costs and better manufacturability compared with DFB and other methods. The ideal spectral manipulation can be realized by a low density of perturbations (slots) of the effective refractive index. It has been proved that the spectrum characteristics can be noticeably improved. A typical spectral width (FWHM) is less than 0.4 nm, and the thermal shift of the spectrum is reduced from 0.26 to 0.07 nm/℃ over the temperature range 0 to 60 ℃.

Acknowledgements

The authors thank S. O'Brien for helpful advice by email. Thanks also to Hu Chuanxian, Fan Zhongchao, Chen Yanling, Yang Xiang, Han Weihua and Ji An in the Engineering Research Center for Semiconductor Integrated Technology, the Institute of Semiconductors, CAS for optical lithography and the ICP dry etching processing of sample devices.

References

[1] Sverdlov B, Mohrdiek S, Pawlik S, et al. Emission wavelength stabilization in broad area lasers coupled to fiber Bragg gratings. Proc SPIE, 2008, 6876: 68761H

[2] Kozlowski D A, Young J S, England J M C, et al. Singlemode 1.3 μm Fabry–Perot lasers by mode suppression. Electron Lett, 1995, 31(8): 648

[3] Corbett B, McDonald D. Single longitudinal mode ridge waveguide 1.3 μm Fabry–Perot laser by modal perturbation. Electron Lett, 1995, 31(25): 2181

[4] Patcell J, Jones D, Kelly B, et al. Specifying the wavelength and temperature tuning range of a Fabry–Perot laser containing refractive index perturbations. Proc SPIE, 2005, 5825: 1

[5] Corbett B, Percival C, Lambkin P. Multiwavelength array of single-frequency stabilized Fabry–Perot lasers. IEEE J Quantum Electron, 2005, 40(4): 490

[6] O'Brien S, O'Reilly E P. Theory of improved spectral purity in index patterned Fabry–Perot lasers. Appl Phys Lett, 2005, 86: 201101

[7] Hays D C, Cho H, Lee J W, et al. High selectivity inductively coupled plasma etching of GaAs over InGaP. Appl Surf Sci, 2000, 156: 76

[8] Baek I K, Lim W T, Lee J W, et al. Comparison of dry etching of AlGaAs and InGaP in a planar inductively coupled BCl_3 plasma. J Vac Sci Technol B, 2003, 21(6): 2487

[9] Hobson W S, Chen Y K, Wu M C. InGaAs/AlGaAs ridge waveguide lasers utilizing an InGaP etch-stop layer. Semicond Sci Technol, 1992, 7: 1425